Microporous and Mesoporous Materials 285 (2019) 1–12

Contents lists available at ScienceDirect

Microporous and Mesoporous Materials

journal homepage: www.elsevier.com/locate/micromeso

Optimization of gold core-mesoporous silica shell functionalization with TPGS and PEI for cancer therapy

Carolina F. Rodrigues[a], Catarina A. Reis[a,b], André F. Moreira[a], Paula Ferreira[c], Ilídio J. Correia[a,c,*]

[a] CICS-UBI — Centro de Investigação em Ciências da Saúde, Universidade da Beira Interior, 6200-506 Covilhã, Portugal
[b] UCIBIO, REQUIMTE — Departamento de Química, Faculdade Ciências e Tecnologia, Universidade Nova de Lisboa, 2829-516 Caparica, Portugal
[c] CIEPQF — Departamento de Engenharia Química, Universidade de Coimbra, Rua 13 Sílvio Lima, 3030-790 Coimbra, Portugal

ARTICLE INFO

Keywords:
Gold core silica shell nanorods
TPGS
PEI
Photothermal therapy
Cancer

ABSTRACT

Photothermal therapy (PTT) has captured the attention of different researchers around the world, since the application of NIR light responsive-nanomaterials has shown promising results in cancer therapy. Gold-core mesoporous silica shell (Au-MSS) nanoparticles allow the combination of gold mediated PTT with the drug delivery in order to improve their therapeutic potential. In this study, two different methodologies, electrostatic or chemical linkage, were explored to functionalize Au-MSS nanorods with TPGS and PEI. For that purpose, the TPGS and PEI were chemically coupled to each other or modified with 3-(triethoxysilyl)propyl isocyanate. The produced Au-MSS nanorods display a uniform morphology and a well-defined gold nucleus and silica shell. Further, the particles surface charge was dependent on the synthesis methodology. The particles modified by electrostatic interactions (Au-MSS/TPGS-PEI) were slightly negative (−16.9 and −5.1 mV) whereas the formulations produced by chemical linkage (Au-MSS/TPGS/PEI) resulted in positively charged nanoparticles (30.9 and 6.8 mV). The successful incorporation of the polymers was confirmed by Fourier Transformed Infrared spectroscopy and thermogravimetric analysis. Moreover, the Au-MSS functionalization did not affect the particles PTT capacity. However, the Au-MSS/TPGS/PEI nanorods displayed a decreased drug encapsulation efficiency. *In vitro* assays demonstrated the cytocompatibility of Au-MSS up to concentrations of 200 μg/mL, however the positively charged formulations only remained biocompatible until 100 and 125 μg/mL. Overall, the attained data confirm the successful modification of Au-MSS nanorods with TPGS and PEI as well as their applicability as PTT and drug delivery agents.

1. Introduction

Cancer is a major health issue and is responsible for millions of deaths worldwide [1]. Chemotherapy, radiotherapy and surgical removal remain as the most commonly used treatments for cancer, however these therapies lack of selectivity and present diverse side effects [2,3]. Therefore, novel anticancer therapeutic approaches are currently under investigation, such as immunotherapy [4] and hyperthermia-based treatments [5]. Hyperthermia comprises a tissue temperature increment, up to 39.5–43 °C, in order to damage or even kill the cancer cells by promoting denaturation of proteins and the disruption of the cell membrane [6]. The temperature increase can be mediated by nanomaterials that are able to accumulate preferentially in the tumor tissue and produce heat in response to specific stimuli, such as magnetic field and near-infrared (NIR) radiation (*i.e.* photothermal effect) [7,8]. So far, several NIR light-responsive nanomaterials, such as graphene oxide [9], gold [10], polymers [11] and small molecules (*e.g.* IR780) [12], have been developed and applied as photothermal agents. Gold nanoparticles are especially promising devices for photothermal therapy (PTT) due to their surface plasmon resonance oscillation which renders them a strong absorption on the NIR region. Further, gold material is bioinert and presents a high flexibility in terms of shape, size, and surface chemistry [13–15]. Moreover, gold nanoparticles can also act as imaging agents for computed tomography, magnetic resonance and photoacoustic imaging, which allow their use in the real-time monitoring of the therapeutic response as well as the nanoparticles traffic in the human body [16–19]. However, when bare gold nanoparticles are in contact with biological fluids they tend to aggregate since they are prone to interact with proteins [20,21]. In addition, the irradiation of gold nanoparticles with NIR light can compromise their

* Corresponding author.CICS-UBI - Centro de Investigação em Ciências da Saúde, Universidade da Beira Interior, Avenida Infante D. Henrique, 6200-506, Covilhã, Portugal.
E-mail address: icorreia@ubi.pt (I.J. Correia).

https://doi.org/10.1016/j.micromeso.2019.04.064
Received 26 November 2018; Accepted 24 April 2019
Available online 28 April 2019
1387-1811/

physical integrity due to the heat-mediated nanoparticle reshaping [22–24]. Thus, the integrity and biocompatibility of the gold nanoparticles decrease as well as their therapeutic potential [22–24]. To overcome these drawbacks, the gold nanoparticles post-synthesis modification with different coating materials, such as dextran, poly (isobutylene-alt-maleic anhydride)-graft-dodecyl, poly(ethylene glycol) and mesoporous silica, has been widely explored [25–29]. Among them, the mesoporous silica coating of gold nanoparticles (Au-MSS) displays promising properties for cancer therapy and imaging [30,31]. Mesoporous silica presents an improved biocompatibility and a large surface area that can be easily modified with various groups such as stealthing agents and targeting moieties [32,33]. Further, silica is optically transparent to NIR light and therefore do not compromise the PTT capacity of the gold core [34,35]. In fact, the inclusion of the silica shell avoids the gold core degradation upon irradiation with the NIR light [36,37]. Moreover, the tubular pores of mesoporous silica allow the encapsulation of drugs and therefore the combination of PTT with chemotherapy towards a synergistic therapeutic effect [33,38]. However, it is necessary to avoid the premature drug leakage from the nanoparticles and increase their blood circulation time to further enhance the therapeutic outcome [39,40].

Herein, D-α tocopherol polyethylene glycol 1000 succinate (TPGS) and branched Polyethylenimine (PEI) were combined for the first time to functionalize Au-MSS nanorods. For that purpose, two different synthesis procedures were performed comprising the chemical linkage of the polymers onto the particles surface or the electrostatic bonding of the TPGS-PEI co-polymer through a simple vortex method. Au-MSS nanorods were produced with different polymer ratios and their physicochemical properties as well as cytocompatibility were characterized to select the most promising nanoparticle formulations. TPGS, a water-soluble vitamin E derivative, was selected based on its amphiphilic nature that can at as solubilizer and consequently increase the colloidal stability of these nanorods [12,41,42]. In addition, TPGS can also act as an inhibitor of P-gp, a drug efflux pump overexpressed in cancer cells, and therefore improve the bioavailability of the chemotherapeutics [42,43]. On the other side, PEI is a cationic polymer routinely used to bind negatively charged cargos [44]. In these nanorods, PEI will be attracted to the negatively charged mesoporous silica surface blocking the particle pores and consequently the drug release.

2. Materials and methods

2.1. Materials

Hydrogen tetrachloroaurate (III) hydrate ($HAuCl_4$) was purchased from Alfa Aesar (Karlsruhe, Germany). Tetraethylorthosilicate (TEOS) and tetrahydrofuran (THF) were obtained from Acros Organics (Geel, Belgium). Hexadecyltrimethylammonium bromide (CTAB) was acquired from Tokyo Chemical Industry (Tokyo, Japan). Hydrochloric acid (HCl) was purchased to Panreac (Barcelona, Spain). Methanol was obtained from VWR International (Carnaxide, Portugal). L-ascorbic acid (AA), silver nitrate ($AgNO_3$), Dulbecco's Modified Eagle medium-high glucose (DMEM-HG), ethanol (EtOH), ethylenediamine tetraacetic acid (EDTA), Fluorescein 5-isothiocyanate (FITC), resazurin, sodium borohydride ($NaBH_4$), Paraformaldehyde, Phosphate-buffered saline (PBS) solution, D-α tocopheryl polyethylene glycol 1000 succinate (TPGS) (Mw ~ 1513 g/mol), Triton-X, 1,1′-Carbonyldiimidazole (CDI), Branched Polyethylenimine (PEI) (Mw ~ 1250 g/mol, ρ = 1.08 g/mL), 3-(Triethoxysilyl)propyl isocyanate (TESPIC), Toluene and trypsin were bought from Sigma-Aldrich (Sintra, Portugal). Human negroid cervix epithelioid carcinoma (HeLa) cells (ATCCs CCL-2t) were acquired from ATCC (Middlesex, UK). Fetal bovine serum (FBS) was acquired to Biochrom AG (Berlin, Germany). Wheat germ agglutinin conjugate Alexa 594® (WGA-Alexa Fluor 594®) and Hoechst 33342® were purchased from Invitrogen (Carlsbad). Doxorubicin hydrochloride (Dox) was obtained from Carbosynth (Berkshire, UK). Cell imaging plates were acquired from Ibidi GmbH (Ibidi, Munich, Germany). Cell culture t-flasks were supplied by Orange Scientific (Braine-l'Alleud, Belgium).

2.2. Synthesis of Au–MSS rods

The nanorods were synthesized through a method comprised of 3 main steps, as previously described in the literature [45]. In the first step, a seed solution was prepared through the addition of 0.6 mL of $NaBH_4$ (0.01 M) under magnetic stirring, to an aqueous solution with 5 mL of CTAB (0.2 M) and 5 mL of $HAuCl_4$ (0.0005 M). After 6 h at 30 °C, the seed solution was added to a growth solution, which was prepared by adding under magnetic stirring 0.03 mL of $AgNO_3$ (0.1 M), 0.3 mL of $HAuCl_4$ (0.05 M) and 0.21 mL of AA (0.08 M) to an aqueous solution containing 20 mL of CTAB (0.2 M). The resulting solution was then left undisturbed for 16 h, at 30 °C, to promote the formation of gold nanorods.

The synthesis of mesoporous silica shell was carried out by adapting the method described by Dias and co-workers [10]. Initially, the gold nanorods were centrifuged (12,000 g, for 20 min at 25 °C) in order to remove the excess of CTAB, and resuspended in 10 mL of ultrapure water. Then 0.7 mL of CTAB (0.01 M) was added and left under stirring overnight at 40 °C. Afterward, 0.07 mL of NaOH (0.1 M) was added to the solution and mixed over 30 min. Then 0.03 mL of a solution of TEOS (20% V/V) in methanol were added. This step was repeated three times, with intervals of 30 min, and the solution was left under stirring for 24 h at 40 °C. The final solution was centrifuged (12,000 g, for 25 min at 25 °C) and washed with ultrapure water in order to recover the Au-MSS nanorods.

2.3. Removal of the surfactant template

The removal of surfactant (CTAB) from Au-MSS nanorods was performed through a solvent based approach described in the literature by Moreira and co-workers [46]. The nanoparticles were resuspended in an acidic solution (HCl 5% v/v in EtOH), sonicated for 2 min, and centrifuged (18,000 g for 15 min at 4 °C). This step was repeated several times, followed by 2 washes in both EtOH (99.9% v/v) and ultrapure water. The final product was centrifuged and resuspended in ultrapure water.

2.4. Synthesis of TPGS-PEI branched co-polymer and TPGS-TESPIC and PEI Branched-TESPIC derivatives

TPGS-PEI Branched co-polymer was synthesized through a method previously described elsewhere [47,48]. Briefly, TPGS (100 mg) was dissolved in 20 mL of dried toluene, under a nitrogen atmosphere, for 6 h at room temperature. Then TPGS was activated with 1,1′-carbonyldiimidazole (CDI) (24 mg) and mixed over 24 h, under nitrogen atmosphere. Afterward, branched PEI (0.1 mL) was added to the activated TPGS and left under stirring for 24 h. After the reaction time, the solvent was evaporated (Rotavap®R-215, Büchi, Switzerland) and the remaining film was hydrated with ultrapure water, sonicated, dialyzed and then recovered by freeze-drying. In order to allow the chemical linkage of TPGS and PEI to the Au-MSS nanorods, the polymers were modified with TESPIC by adapting a method previously described in the literature [49,50]. Briefly, TPGS (500 mg) or PEI (0.1 mL) were dissolved in 20 mL of THF under a nitrogen atmosphere and magnetic stirring, for 6 h at room temperature. Subsequently, TESPIC was added to the polymer solution and left to react for 24 h. Thereafter, the solvent was evaporated (Rotavap®R-215, Büchi, Switzerland) and the remaining film was hydrated with ultrapure water, sonicated, dialyzed and freeze-dried. The successful modification of TPGS and PEI Branched polymers was assessed by performing the Fourier Transform Infrared (FTIR) analysis of the samples.

2.5. Au-MSS functionalization

The polymer functionalization of Au-MSS was performed using two different methodologies. In the first approach, TPGS-PEI Branched co-polymer was used to modify the nanorods by promoting electrostatic interactions between the negatively charged mesoporous silica surface and the positively charged amine groups on PEI. For that purpose, 5 mg of nanoparticles were resuspended on TPGS-PEI Branched co-polymer solution (5 mg/mL). Then, this solution was vortexed for 1 min or 5 min and the particles (Au-MSS/TPGS-PEI) recovered by centrifugation (4,000 g for 20 min at 25 °C) and washed to remove the polymer excess.

Alternatively, TPGS and PEI polymers were chemically linked to the Au-MSS surface by using a post-synthesis grafting methodology, as previously described in Ref. [51]. Briefly, Au-MSS nanorods (20 mg) were resuspended in 40 mL of EtOH (33%, pH 4), and sonicated for 5 min. Then, TPGS-TESPIC and PEI-TESPIC polymers were added to the nanoparticles solution (ratio 1:1 or 3:1 w/w). After 24 h, the final solution was centrifuged (8,000 g, for 25 min at 25 °C) and washed several times with ultrapure water to recover the Au-MSS/TPGS/PEI nanorods and remove the solvent.

2.6. Characterization of nanocarriers' physicochemical properties

The morphology of both coated and uncoated Au-MSS rods was characterized by Transmission Electron Microscopy (TEM – Hitachi-HT7700, Japan). The nanoparticles samples were placed on formvar-coated copper grids and dried at 25 °C, and then the images were acquired at accelerating voltage of 100Kv. After that, nanoparticles total size, silica shell thickness, and gold core size were measured by software (Image J 2.0.0, NIH Image, USA). The success of the Au-MSS nanorods purification process as well as their functionalization with the polymers was accessed by acquiring the FTIR spectra of the nanoparticles on a Nicolet iS10 spectrometer, with a 4 cm^{-1} spectral resolution from 600 to 4,000 nm (Thermo Scientific Inc., Massachusetts, USA). The polymer content on the Au-MSS formulations was measured by performing the thermogravimetric analysis (TGA) of the samples. Briefly, uncoated or coated Au-MSS rods were heated up to 600°C, at a heating rate of 10°C/min under an inert atmosphere on a SDT Q600 equipment (TA Instruments, USA), and the particles' weight losses were recorded along time.

The Au-MSS, Au-MSS/TPGS-PEI and Au-MSS/TPGS/PEI nanorods NIR absorption capacity was evaluated through the acquisition of the particles' UV–vis spectra using an UV–vis spectrophotometer (Thermo Scientific Evolution™ 201 Bio UV–vis Spectrophotometer, Thermo Fisher Scientific Inc., USA) at a 300 nm min^{-1} scanning rate, with a wavelength range from 200 to 1,100 nm. The zeta potential of coated and uncoated nanoparticles was determined by using a Zetasizer Nano ZS equipment (Malvern Instruments, Worcestershire, UK).

2.7. In vitro photothermal measurements

The evaluation of the *in vitro* photothermal capacity of coated and uncoated Au-MSS was performed as described in the literature [10]. Thus, nanoparticles at different concentrations (50, 100 and 200 μg/mL) and a control group with particles were irradiated with a NIR laser light (808 nm, 1.7 W/cm^2). The temperature variation of the solution was measured at different time points (from 1 up to 10 min) by using a thermocouple sensor with an accuracy of 0.1 °C.

2.8. Drug loading

The Dox loading on coated or uncoated Au-MSS rods was performed through the impregnation of the particles in a Dox solution, as previously described by Dias and co-workers [45]. Briefly, the Au-MSS were resuspended in 5 mL of methanol containing Dox (40 μg/mL), and sonicated for 15 min. Then, the solution was mixed under stirring for 48 h at room temperature. After that, the drug-loaded nanoparticles were recovered by centrifugation (18,000 g for 20 min at 4 °C) and freeze-dried. The supernatant was used to quantify the amount of drug loaded within nanoparticles. Thus, the Dox content was calculated by measuring the supernatant absorbance at 485 nm (Thermo Scientific Evolution 201 Bio UV–vis Spectrophotometer, Thermo Fisher Scientific Inc., USA), and using a calibration curve (ABS = 16.715C-0.0006; R^2 = 0.9971). The encapsulation efficiency was calculated through equation (1):

$$\text{Encapsulation efficiency (\%)} = \frac{\textit{Initial drug weight} - \textit{Drug weight present in the supernatant}}{\textit{Initial drug weight}} \text{x100} \quad \text{Eq.(1)}$$

2.9. Cytocompatibility assays

2.9.1. Cell viability

The cytocompatibility of coated and uncoated Au-MSS nanorods was evaluated through a resazurin-based assay [52]. Briefly, HeLa cells were seeded into 96-well flat bottom culture plates at a density of 10,000 cells per well with 200 μl of DMEM-HG medium. During approximately 24 h, cells were cultured at 37 °C in a humid atmosphere containing 5% CO_2. Afterward, cells were cultured with different concentrations (25–200 μg/mL) of Au-MSS, Au-MSS/TPGS-PEI or Au-MSS/TPGS/PEI. After 24 and 48 h of incubation, the medium was replaced and cells were incubated with 10%(v/v) of resazurin(1 mg/mL), at 37 °C and 5% CO_2 during 4 h. The produced resorufin present in the medium was quantified by using a microwell plate reader (Spectramax Gemini XS, MolecularDevices LLC, USA) at an excitation/emission wavelength of λex = 560 nm and λem = 590 nm. Cells cultured in the absence of nanoparticles were used as negative control (K^-), whereas cells incubated with EtOH (99.9%) were used as positive control (K^+).

2.9.2. Evaluation of the Au–MSS effects on cells' migration ability

The wound closure assay was performed to evaluate the nanoparticles influence in the HeLa cells' migration ability [10]. For that purpose, HeLa cells were seeded on 12-well flat bottom culture plates at a density of 50,000 cells per well, with 2 mL of medium. Cells were maintained in culture (at 37 °C, in a humid atmosphere with 5% CO_2), until reaching confluence. After this period, the medium was removed and a gap was made by using a micropipette tip. Then, cells were incubated with 100 μg/mL of the different Au-MSS formulations, during 24 and 48 h. A control group without particles was also monitored. Images were captured by using an Olympus CX41 inverted optical microscope equipped with an Olympus SP-500 UZ digital camera, and the cells' migration distance was measured using Image J software (Image J 2.0.0, NIH Image, USA).

2.9.3. Hemolysis assay

The hemolysis experiments were also performed to evaluate the Au-MSS nanoformulations impact on blood hemolysis [53]. Briefly, blood samples freshly obtained from adult mice, were stabilized with EDTA. Then, the whole blood samples were centrifuged at 500 g, for 5 min, at 4 °C in order to recover the red blood cells (RBCs). After that period, the RBCs were washed three-times with NaCl solution (150 mM), diluted in PBS, distributed by the test tubes, and centrifuged. Afterward, 1 mL of PBS solution containing coated or uncoated Au-MSS nanorods at different concentrations (100, 150, and 200 μg/mL) were added to the RBC suspension and were incubated at room temperature for 2 and 4 h. At the same time, the negative (K^-) and positive (K^+) control were prepared by adding 1 mL of PBS and Triton-X 100, respectively. All the samples were slightly shaken once for every 30 min to resuspend the RBCs and particles. After the incubation period, the samples were centrifuged at 500 g for 5 min, at 4 °C and 100 μL of supernatants were

transferred to a 96-well plate to measure the hemoglobin absorbance at 570 nm. RBCs hemolysis percentage was calculated through equation (2):

$$\text{Hemolysis (\%)} = \frac{\textit{Sample Abs} - \textit{Negative Control Abs}}{\textit{Positive Control Abs} - \textit{Negative Control Abs}} \quad \text{Eq.(2)}$$

2.10. Evaluation of the nanoparticle' cellular uptake

The Au-MSS formulations uptake by HeLa cells was characterized through confocal laser scanning microscopy (CLSM) following a protocol previously described by Gaspar and co-workers [54]. For this purpose, the different Au-MSS nanorods formulations were labelled with FITC. For the analysis of the nanoparticles cellular uptake, 15,000 HeLa cells were seeded in μ-Slide 8 well Ibidi imaging plates and incubated for 48 h, at 37 °C and 5% CO_2. Afterward, cells were incubated with 200 μg/mL of Au-MSS formulations for 4 h. Subsequently, the seeded cells were washed with PBS, fixed with paraformaldehyde (4% w/v) for 10 min and rinsed with PBS. For cell nucleus staining, cells were treated with Hoechst 33342®, whereas the cytoplasm of the cells was labelled with WGA-Alexa Flour 594®. The CLSM images were then acquired with a Zeiss LSM 710 Confocal microscope (Carl Zeiss SMT Inc., Germany) equipped with a Plan Apochromat 63x/1.4 Oil Differential Interference Contrast objective.

2.11. Statistical analysis

All data are presented as mean ± standard deviation (s.d.). Oneway analysis of variance (ANOVA) with the Student–Newman–Keuls post-test was used for multiple groups comparison. A p-value lower than 0.05 ($p < 0.05$) was considered to be statistically significant. Statistical analysis was performed using GraphPad Prism v.6.0 software (Trial version, GraphPadSoftware, CA, USA).

3. Results and discussion

3.1. Synthesis and characterization of TPGS-PEI, TPGS-TESPIC and PEI-TESPIC polymers

TPGS and PEI were chemically modified to allow the posterior functionalization of the Au-MSS nanorods. Two different modifications were investigated, the TPGS linking to PEI through a CDI-mediated coupling reaction (TPGS-PEI co-polymer) [47,48] and the individual modification of TPGS and PEI with TESPIC (TPGS-TESPIC and PEI-TESPIC silane derivatives) through hydrogen-transfer nucleophilic addition reaction [49,50] (Fig. 1A). The modification of the TPGS-PEI, TPGS-TESPIC and PEI-TESPIC was confirmed through FTIR analysis (Fig. 1B). The FTIR spectra of TPGS and TPGS-PEI co-polymer shows the TPGS characteristic peaks at 1,740 cm^{-1} and 1,105 cm^{-1} corresponding to the vibration peak of C═O bond and C—O stretching vibration, respectively [55]. Further, due to the inclusion of the PEI chain it is also possible to observe the changes in the ratio between the peaks at 1,146 cm^{-1} and 1,052 cm^{-1}, which are attributed to the vibration of the PEI C—N bonds that also occur in the 1145 cm^{-1} region. The TPGS-TESPIC spectrum showed a distinctive absorption peak in the 1,680-1,640 cm^{-1} region assigned to the newly formed secondary amides. Moreover, the introduction of the silane moiety on the TPGS backbone also changed the spectrum in the 1,110-1,050 cm^{-1} region due to the absorption band of the Si—O—C bonds. Similar results were obtained for the PEI-TESPIC derivative, where it is possible to identify an absorption band on the 1,110-1,050 cm^{-1} region attributed to the Si—O—C bonds, indicating the successful PEI modification with the TESPIC.

3.2. Synthesis and characterization of Au-MSS nanorods

The Au-MSS rods were synthesized by using a seed-mediated methodology [10,56,57]. The synthesis method involved three main steps: production by nucleation of small spherical gold particles, that are then added to a growing solution to form the gold nanorod, and finally the production of the mesoporous silica shell coating using CTAB as a soft template to generate the pores. The successful synthesis of Au-MSS nanorods, with homogeneous distribution and organized in a single gold-core with a uniform silica shell, was confirmed via TEM images (please see figure S1). The TEM images show that the gold-core present a mean length and width of 43 ± 8 nm and 14 ± 3 nm, respectively, corresponding to an aspect ratio (AR) of 3.1. Moreover, the Au-MSS nanorods presented a mean mesoporous silica shell thickness of 22 nm resulting in particles with a total length and width of 84 ± 10 and 60 ± 4 nm, respectively (Fig. 2A). The obtained gold-core AR is compatible with the Au-MSS nanorods application in NIR-mediated PTT applications [58,59]. In fact, ARs between 3 and 4 have been reported has optimal to absorb the NIR light [58,60]. On the other side, the Au-MSS overall size still allows them to exploit the enhanced permeability and retention effect and therefore to accumulate passively in the tumor tissue [49]. The successful removal of the cytotoxic CTAB molecules from the Au-MSS was confirmed through FTIR (Fig. 2C). The Au-MSS nanorods spectra does not contain the two characteristic bands of CTAB, between 2,950 cm^{-1} and 2,850 cm^{-1}, which correspond to the C—H vibration, and 1,450-1,500 cm^{-1}, that is attributed to CH_3—N^+ deformation [10]. In addition, it is possible to observe the mesoporous silica shell characteristic peaks in the 1,100 to 750 cm^{-1} region, that correspond to Si—O—Si, Si—O and Si—OH vibrations [52]. Therefore, this data indicates the successful purification of Au-MSS nanorods.

3.3. Synthesis and characterization of Au-MSS/TPGS-PEI and Au-SS/TPGS/PEI nanoparticles

The Au-MSS nanorods were functionalized using two different approaches, through electrostatic interaction or by chemical linkage through a post-synthesis grafting methodology (figure S2). The first approach is based on the establishment of the electrostatic interactions between the negatively charged surface of Au-MSS nanorods and positively charged amine groups on TPGS-PEI co-polymer. The chemical linkage was performed by promoting the grafting of the TPGS-TESPIC and PEI-TESPIC silane derivatives on the surface of the Au-MSS nanorods (figure S1 B, C, and D).

The Au-MSS nanorods surface functionalization was confirmed by measuring the zeta potential (Fig. 2B). The Au-MSS nanorods displayed a negative surface charge, −24.3 ± 3.7 mV, attributed to the presence of negatively charged silanol groups on the mesoporous silica surface. The Au-MSS/TPGS-PEI nanoparticles surface charge was dependent on the vortex time, the particles vortexed for 1 min presented a zeta potential of −5.1 ± 0.2 mV. Further, the increase in the vortex time to 5 min resulted in a more negative zeta potential, −16.9 ± 0.6 mV, which indicates a lower efficacy on functionalizing the particle surface. On the other side, the Au-MSS nanorods functionalized with TPGS/PEI (ratio 1:1) presented a zeta potential of 30.9 ± 5.7 mV, whereas the increase of the TPGS content (ratio 3:1) provoked a decrease on the surface charge to 6.8 ± 1.2 mV. Therefore, these results confirm the polymers binding to the Au-MSS surface, since the changes observed on the surface charge are explained by the positively charged amine groups present on the PEI. Additionally, in the Au-MSS/TPGS/PEI (3:1), the reduction on the surface charge may also indicate a reduction of the amount of PEI chains grafted on the particle surface.

As described in the literature, the nanoparticles pharmacokinetic profile, blood circulation time and biocompatibility are highly influence by their surface charge [61,62]. In fact, a neutral surface charge (± 10 mV) is until now considered the ideal for nanoparticles circulation, whereas slightly positive particles often present a higher

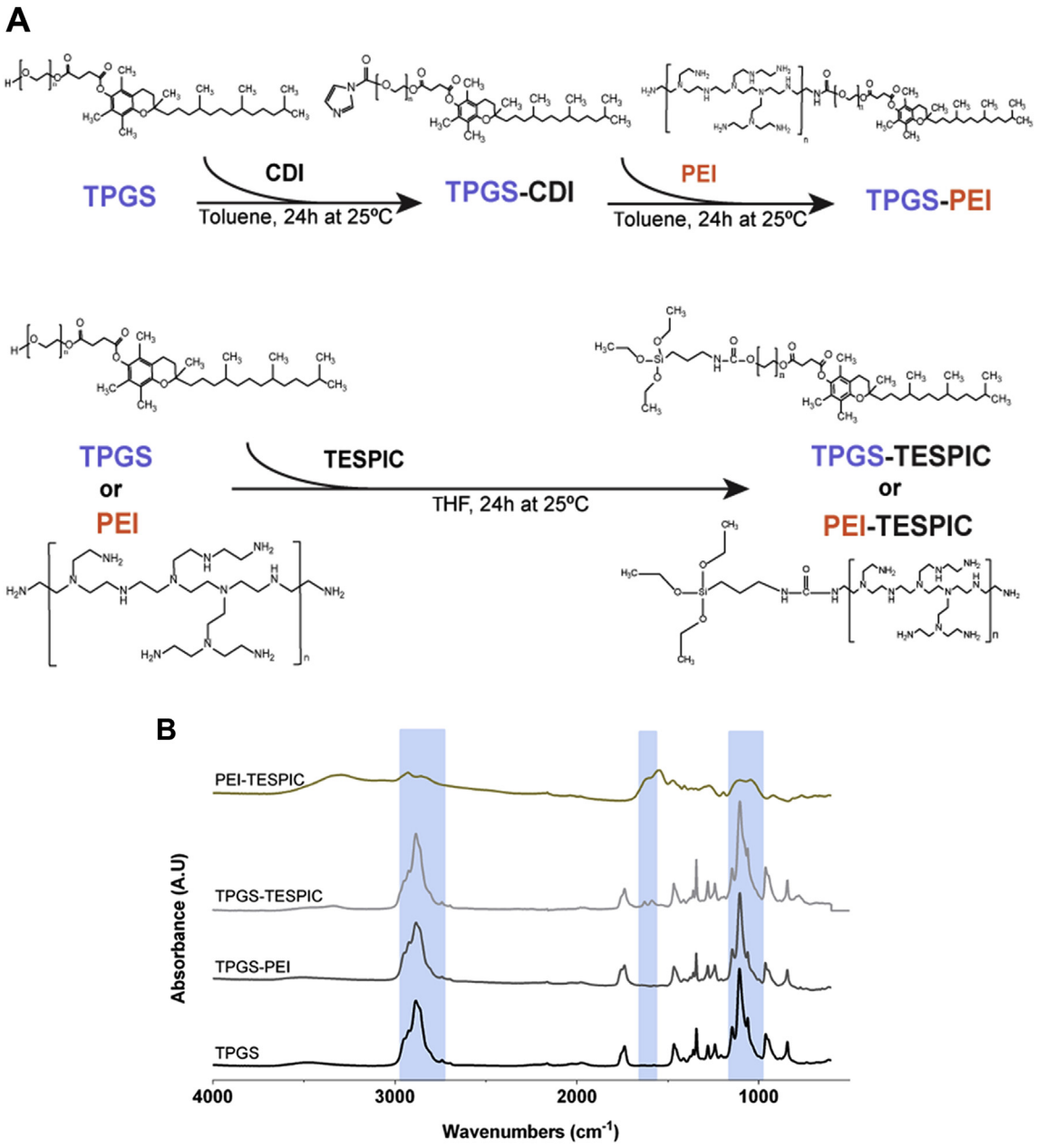

Fig. 1. Synthesis of TPGS-PEI, TPGS-TESPIC and PEI-TESPIC polymers. (A) Schematic of the synthesis of polymers. (B) FTIR spectra of TPGS, TPGS-PEI, TPGS-TESPIC and PEI-TESPIC.

internalization by the cells [63,64]. Taking this into account, only the Au-MSS/TPGS-PEI 1 min, Au-MSS/TPGS/PEI (1:1) and Au-MSS/TPGS/PEI (3:1) formulations were selected for the subsequent studies. The Au-MSS nanorods modification with the polymers was further confirmed by FTIR (Fig. 2C). The Au-MSS/TPGS-PEI 1 min spectra showed the characteristic peaks of the silica shell on the 1,100 to 750 cm^{-1} region and additionally, the presence of peaks at 2,900 cm^{-1} and 1,700 cm^{-1} regions assigned to the TPGS and PEI, respectively. Similar results were observed on the Au-MSS/TPGS/PEI (1:1) and Au-MSS/TPGS/PEI (3:1) formulations. Moreover, the successful grafting of the silane modified polymers on the surface of nanorods was also confirmed by the increase of the ratio between the Si—O—Si peak at 1,045 cm^{-1} and Si—OH peak at 950 cm^{-1}. Additionally, the Au-MSS nanorods polymer content was determined by performing a thermogravimetric analysis (Fig. 2D). The weight losses observed for Au-MSS nanorods were minimal and can be attributed to the evaporation of water in the interior of the mesopores and to the loss of the functional hydroxyl groups on the surface of the particles [65,66]. On the other side, the recorded weight losses were superior for the Au-MSS/TPGS-PEI, Au-MSS/TPGS/PEI (1:1) and Au-MSS/TPGS/PEI (3:1), which is attributed to the polymers pyrolysis and corroborates the successful functionalization of the nanorods by both methodologies. The calculated polymer content for Au-MSS/TPGS-PEI, Au-MSS/TPGS/PEI (1:1) and Au-MSS/TPGS/PEI (3:1) was 12%, 10% and 25%, respectively. The increase of the polymer content with the increase of the TPGS/PEI ratio on Au-MSS/TPGS/PEI (1:1) and Au-MSS/TPGS/PEI (3:1) nanorods may be justified by a reduction of the electrostatic repulsion between the PEI chains, thus favouring the polymer grafting on the particles surface.

3.4. Drug loading capacity of Au-MSS derivatives

The Au-MSS capacity to encapsulate chemotherapeutic drugs was characterized by measuring the encapsulation efficiency of Dox. The Dox loading was promoted by resuspending Au-MSS nanoparticles (*i.e.*

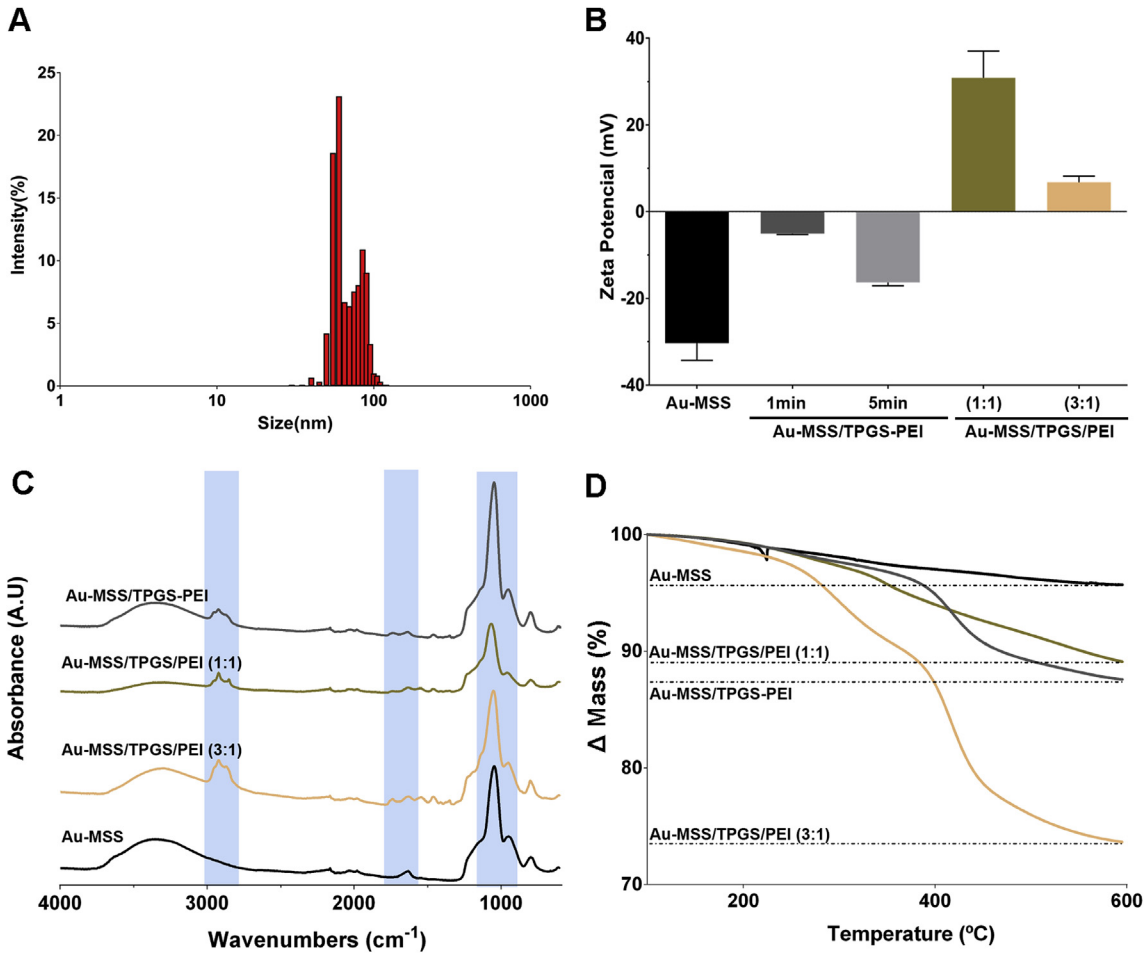

Fig. 2. Physicochemical characterization of Au-MSS derivatives. (A) Au-MSS size distribution (length and width included), n = 300. (B) Surface charge analysis of Au-MSS, Au-MSS/TPGS-PEI and Au-MSS/TPGS/PEI formulations, n = 3. (C) FTIR spectra of Au-MSS, Au-MSS/TPGS/PEI (3:1), Au-MSS/TPGS/PEI (1:1) and Au-MSS/TPGS-PEI (1 min). (D) TGA analysis of Au-MSS, Au-MSS/TPGS/PEI (1:1), Au-MSS/TPGS/PEI (3:1) and Au-MSS/TPGS-PEI (1 min).

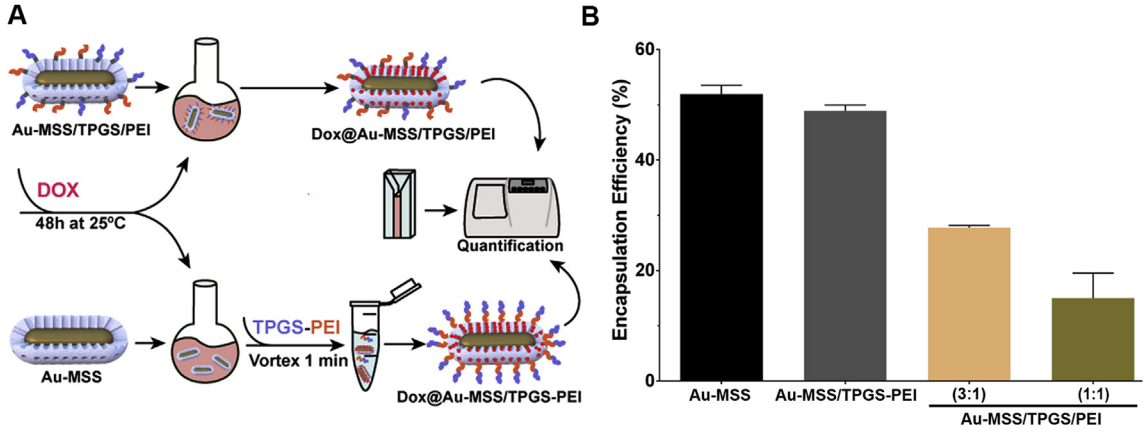

Fig. 3. Characterization of Dox encapsulation efficiency. (A) Schematics of the two methodologies of drug loading for Au-MSS/TPGS/PEI and Au-MSS/TPGS-PEI formulations. (B) Dox encapsulation efficiency on Au-MSS, Au-MSS/TPGS-PEI (1 min), Au-MSS/TPGS/PEI (3:1) and (1:1) nanorods. Data are presented as mean ± s.d., *p < 0.05, n = 3.

Au-MSS and Au-MSS/TPGS/PEI) in Dox solution for 48 h. For the Au-MSS/TPGS-PEI nanorods, the loading was performed before the Au-MSS functionalization with the TPGS-PEI co-polymer (Fig. 3A). The obtained results showed that all the Au-MSS formulations are able to encapsulate Dox (Fig. 3B). Both Au-MSS and Au-MSS/TPGS-PEI nanorods presented an encapsulation efficiency superior to 50% (*i.e.* 10 μg of Dox per Au-MSS mg). This data indicates that no significant drug losses occur during the Au-MSS functionalization with the TPGS-PEI co-polymer. On the other side, the encapsulation efficiency decreased for around 20% on Au-MSS/TPGS/PEI (1:1) and 30% for on Au-MSS/TPGS/PEI (3:1) formulations. This decrease on the encapsulation efficiency can be attributed to blockage of the Au-MSS mesopores by the TPGS and PEI polymers or even to repulsion phenomena between the positively charged PEI chains and Dox molecules.

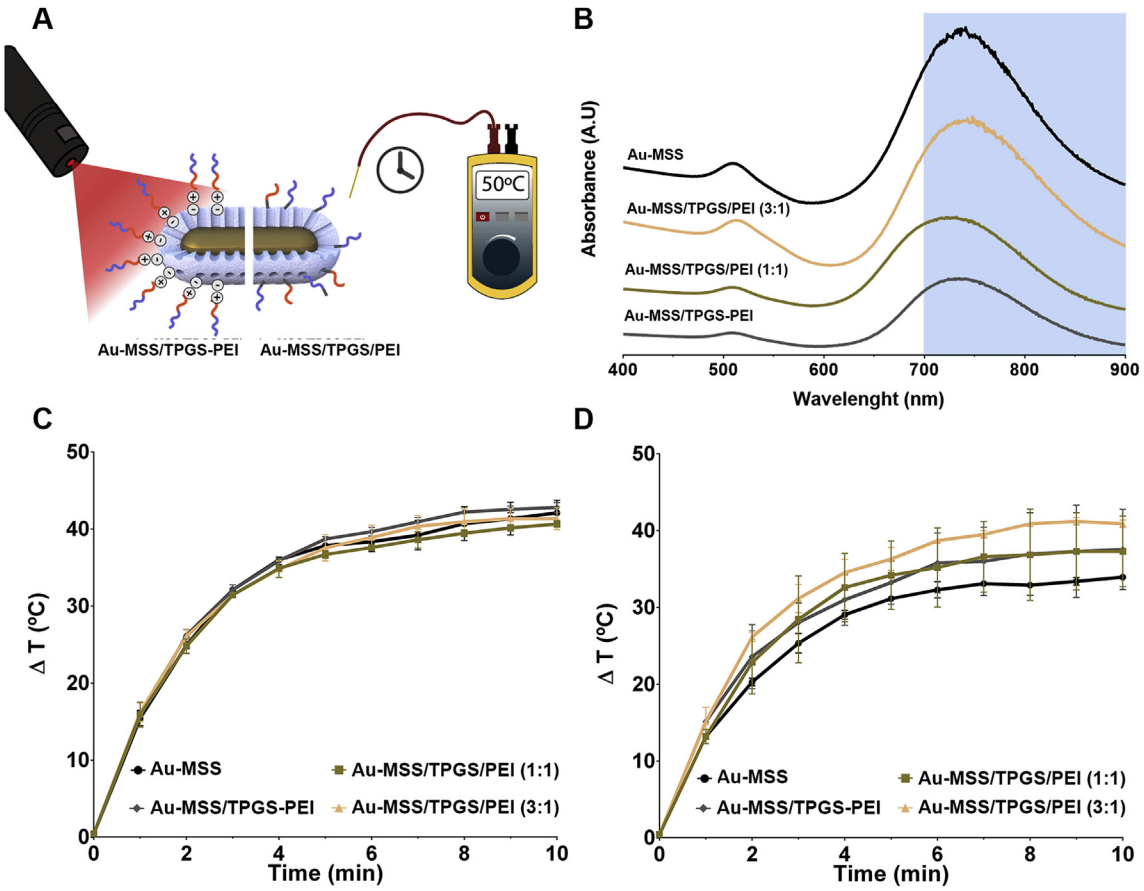

Fig. 4. Characterization of the PTT capacity of Au-MSS nanorods and its derivatives. (A) Schematics of the evaluation of Au-MSS formulations *in vitro* PTT capacity. (B) UV–vis spectra of Au-MSS and derivatives nanorods. (C) Temperature variation curve of Au-MSS derivatives in complex media (DMEM-HG), NIR laser (808 nm, 1.7 W cm^{-2}) irradiation for 10 min. (D) Temperature variation curve of Au-MSS and Au-MSS derivatives in ultrapure water, NIR laser (808 nm, 1.7 W cm^{-2}) irradiation for 10 min. Data are presented as mean ± s.d., *p < 0.05, n = 3.

3.5. In vitro evaluation of the photothermal capacity of nanoparticles

The potential application of Au-MSS derivatives on PTT was firstly assessed by acquiring their UV–Vis–NIR absorption spectrum (Fig. 4B). The Au-MSS nanorods present two characteristics absorption peaks at 515 nm and 750 nm (*i.e.* NIR region) that correspond to the transverse and longitudinal resonances, respectively. Moreover, the functionalization with TPGS-PEI or TPGS-TESPIC and PEI-TESPIC did not induced any significant changes on the absorption capacity of the nanorods. This strong absorption in the 700–900 nm range support the Au—MSS derivatives application in PTT. Further, reduced off-target interactions are expected since the biologic constituents present a low absorption to this radiation [67,68].

After confirming the NIR absorption of Au-MSS derivatives, their capacity to convert optical energy into heat was investigated by measuring the temperature changes induced by the nanoparticles upon NIR laser irradiation (Fig. 4A). In Fig. 4C, it is possible to observe that all the Au-MSS derivatives could induce an increase in the temperature when irradiated with the NIR laser for up 10 min. In addition, the polymers inclusion did not affect the obtained results, being all the formulations capable to produce a temperature variation of about 40 °C. This increase in the temperature can provoke the denaturation of proteins, disruption of cells' membrane, dysfunction of metabolic functions and consequently lead to the cancer cells' death. Further, it is worth to notice that even when this assay was performed in complex media (*i.e.* DMEM-HG medium supplemented with 10% FBS), the performance of the Au-MSS/TPGS-PEI, Au-MSS/TPGS/PEI (1:1) and Au-MSS/TPGS/PEI (3:1) nanorods was not affected (Fig. 4C and D). Such findings, indicate a good particle stability since the particles aggregation can induce changes in the absorption spectra of the nanorods and consequently affect their PTT capacity [69,70].

3.6. Nanoparticles cytocompatibility

3.6.1. Cell viability

The cytocompatibility of non-coated Au-MSS nanorods and its coated derivatives was evaluated on cervical cancer HeLa cells. The different nanoparticles formulations were incubated for 24 and 48 h with HeLa cells, at concentrations ranging from 25 to 200 μg/mL (Fig. 5). The Au-MSS nanorods did not reveal any toxicity towards Hela cells, being registered cell viabilities superior to 70%, even at a concentration of 200 μg/mL. These results are in agreement with different reports available in the literature, where Au-MSS with a rod-like, spherical or other shape were biocompatible with HepG2, HeLa and human dermal fibroblasts [10,71]. Similar results were observed for Au-MSS/TPGS-PEI nanorods. The HeLa cells incubated with Au-MSS/TPGS-PEI (1 min) nanorods at concentrations up to 200 μg/mL presented cell viabilities superior to 80% (Fig. 5B). On the other side, the Au-MSS/TPGS/PEI (1:1) nanoparticles induced a dose-dependent variation on the cell viability of the HeLa cells (Fig. 5C). The cells presented a viability of ~80% at a concentration of 100 μg/mL and continued to decrease to almost 20% with the increase of the nanoparticles concentration up to 200 μg/mL. These results can be explained by the conjugation of the intrinsic anticancer activity of TPGS with the high positive charge density within the PEI chains, which can lead to destabilization of the cell membrane and cellular necrosis [72]. Therefore,

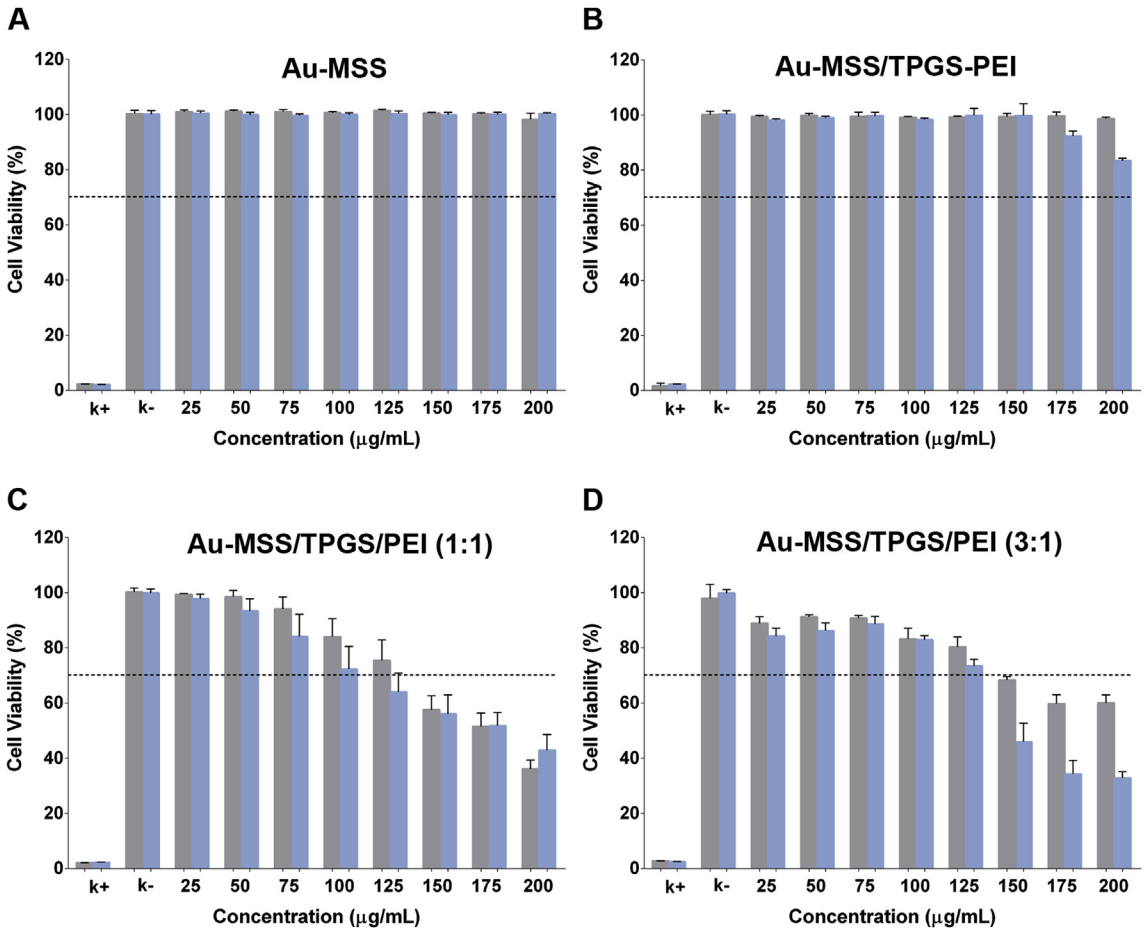

Fig. 5. Evaluation of Au–MSS derivatives cytocompatibility in HeLa cells at 24 and 48 h. (A) Cytocompatibility analysis for Au-MSS, (B) Au-MSS/TPGS-PEI (1 min), (C) Au-MSS/TPGS/PEI (1:1) and (D) Au-MSS/TPGS/PEI (3:1) nanorods. Positive control (K^+): cells treated with EtOH; negative control (K^-): cells without nanoparticles incubation. Data are presented as mean ± s.d., *$p < 0.05$, $n = 5$.

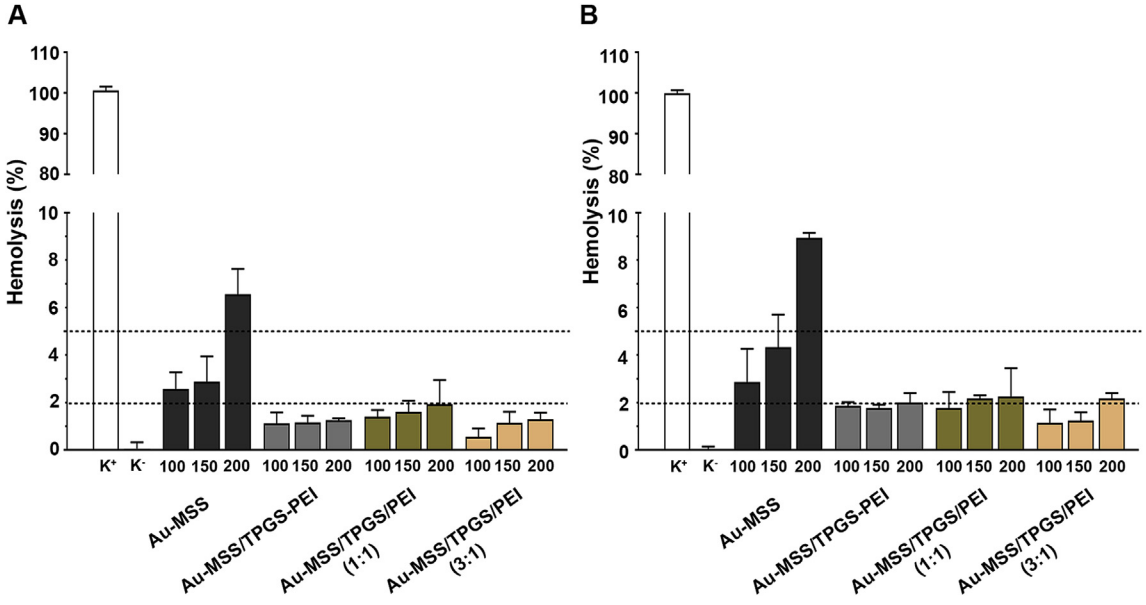

Fig. 6. Analysis of the RBCs lysis upon incubation with 100, 150 and 200 μg/mL of Au-MSS, Au-MSS/TPGS-PEI (1 min), Au-MSS/TPGS/PEI (1:1) and Au-MSS/TPGS/PEI (3:1) nanorods, during 2 (A) and 4 h (B). K^-: RBCs incubated with PBS, K^+: RBC incubated with Triton-X 100. Data are presented as mean ± s.d., *$p < 0.05$, $n = 3$.

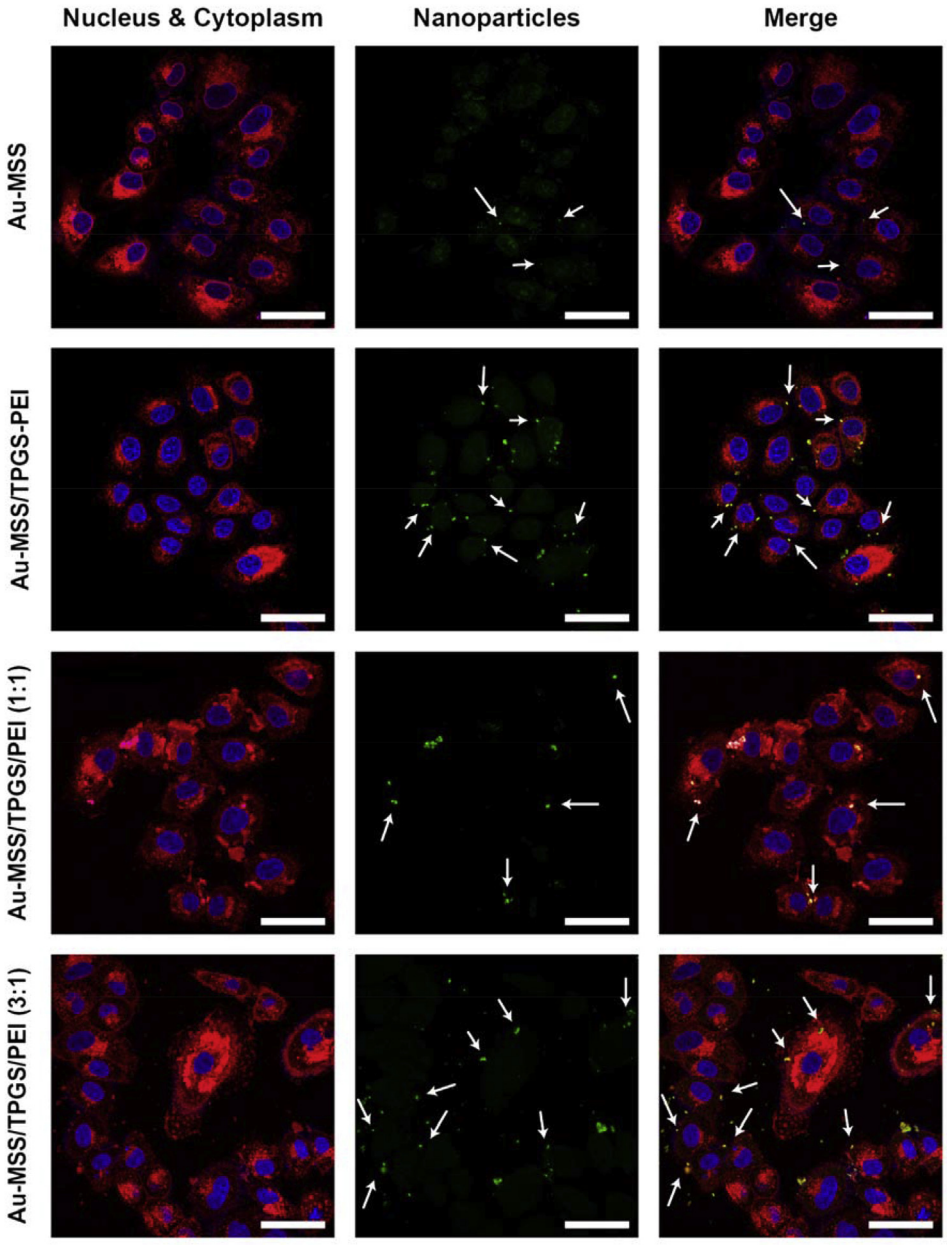

Fig. 7. Representative confocal microscopy images of Au-MSS formulations uptake by HeLa cells. The white arrows are pointing to the internalized nanoparticles. The scale bar corresponds to 50 μm. Blue channel: Hoechst 33342® stained cell nucleus; red channel: WGA-Alexa Fluor 594® stained cell cytoplasm; green channel: FITC labelled nanoparticles. (For interpretation of the references to colour in this figure legend, the reader is referred to the Web version of this article.)

the Au-MSS/TPGS/PEI (3:1) nanoparticles, which presented a neutral surface charge 6.8 mV, displayed a superior cell biocompatibility (Fig. 5D). The results revealed that the HeLa cells treated with Au-MSS/TPGS/PEI (3:1) nanorods up to 125 μg/mL presented cell viabilities superior to 70%.

3.6.2. *Evaluation of the Au-MSS effect on cells' migration ability*

To further characterize the cytocompatibility of the Au-MSS formulations, the nanoparticles effect on the HeLa cells' migration ability was also evaluated (Figure S3 and S4). The obtained results reveal that both Au-MSS and Au-MSS/TPGS-PEI nanorods did not induce any negative effect on HeLa cells motility. In Figure S3 A and B, it is possible to observe that the Control, Au-MSS, and Au-MSS/TPGS-PEI formulations presented almost 45% decrease on the gap width in only 48 h of incubation. These data are in accordance with the previous works were Au-MSS nanorods were reported as being biocompatible even when high concentrations were used [10]. Further, this result also supports the good cytocompatibility demonstrated by Au−MSS/TPGS-PEI nanorods in the cell viability studies. In the other side, the cells treated with Au-MSS/TPGS/PEI nanorods presented a higher gap width (Figure S4 C and D). The Au-MSS/TPGS/PEI (3:1) did not affect the HeLa cells motility when the concentration was inferior or equal to 100 μg/mL, whereas the cells incubated with Au-MSS/TPGS/PEI (1:1) showed an impaired motility even at the lowest tested concentration, i.e. 50 μg/mL. These results confirm the data obtained during the cell viability analysis, where the positive charge of PEI impacts the particles cytocompatibility by promoting the destabilization of the cell membrane and cellular necrosis. Further, similarly to the previously observed, the decrease of the PEI content on the Au-MSS/TPGS/PEI (3:1) formulation also led to a better biological performance.

3.6.3. Hemocompatibility

The TPGS and PEI influence on the Au-MSS cytocompatibility was also evaluated by studying the nanorods hemocompatibility (Fig. 6). In this way, the RBCs lysis upon incubation for 2 and 4 h with the different Au-MSS formulations (100, 150, and 200 μg/mL) was evaluated by UV–vis spectroscopy. The obtained results show that the Au-MSS nanorods are hemolytic at a concentration of 200 μg/mL since more than 5% of hemoglobin was released after 2 and 4 h of incubation. On the other side, all the coated formulations presented a safe hemolytic ratio, ranging the 2% after the 4 h of incubation. These results can be justified by the neutral surface charges of Au-MSS/TPGS-PEI and Au-MSS-TPGS-PEI that decreases its interaction with RBCs, as well as by the increased resistance of healthy cells to the intrinsic activity of TPGS [9]. In fact, Neophytou et al. verified that TPGS could induce the cancer cells death via inhibition of Akt phosphorylation and consequent decrease of BcL-2 and Survivin, whereas normal cells are not affected by this action [72].

3.7. Evaluation of the nanoparticle' cellular uptake

After assessing the cytocompatibility of Au-MSS formulations, the nanoparticles cellular uptake was evaluated by using confocal microscopy. The nanoparticles' cellular uptake is one of the most important barriers that drug delivery systems have to overcome when applied in cancer therapy. In this study, the nanoparticles tracking was achieved by labelling Au-MSS nanorods with FTIC. In Fig. 7, it is possible to observe the internalization of all Au-MSS formulations. These data are in agreement with previous studies where it was demonstrated the nanorods capacity to transpose the cell membrane, even with a superior efficiency than the spherical counterparts [10,73,74]. Additionally, the CLSM images (Fig. 7) also indicate that the functionalization of Au-MSS nanorods with TPGS and PEI improves the nanoparticles' uptake. Despite the differences in the synthesis methodology, the cells treated with Au-MSS/TPGS-PEI and Au-MSS/TPGS/PEI (3:1) present a similar staining by the nanorods, which may be attributed to their neutral surface charge (i.e. −5.1 and + 6.8, respectively) Surprisingly, the Au-MSS/TPGS/PEI (1:1) formulation, which presents a highly positive surface charge, appear to have a lower internalization on HeLa cells than the other coated nanorods. Such result may be explained by the higher PEI content that has been associated with the disruption of the cell membrane and consequent lower cytocompatibility. Altogether, this data indicates that the synthesis methodology used for functionalizing the Au-MSS nanorods, electrostatic interaction or chemical linkage, may not influence the nanoparticles cellular uptake. Further, the Au-MSS/TPGS-PEI and Au-MSS/TPGS/PEI (3:1) formulations were successfully internalized by HeLa cells, which will allow the drug release in cell cytoplasm thus avoiding the premature drug degradation and increasing the therapeutic potential.

4. Conclusion

The Au-MSS nanorods are multifunctional nanomaterials that can act simultaneously as drug delivery, photothermal and bioimaging agents. However, it is essential to improve nanoparticles' circulation time and release profile when biological applications are intended. For that purpose, in this study two different methodologies were explored and optimized to functionalize Au-MSS nanorods with TPGS and PEI in order to increase the colloidal stability of these nanorods and avoid the drug leakage. Polymer coated Au-MSS nanorods were produced by promoting the electrostatic adsorption of TPGS-PEI co-polymer or the chemical grafting of each polymer individually on the particle surface. The obtained results demonstrate that the Au-MSS nanorods functionalization did not impact the nanorods overall size and on their PTT potential. Further, the synthesis methodology and polymer ratio influenced the nanorods surface charge as well as their capacity to encapsulate Dox. The *in vitro* assays, showed that the Au-MSS and Au-MSS/TPGS-PEI were biocompatible at concentrations up to 200 μg/mL, whereas these values were slightly lower for Au-MSS/TPGS/PEI (1:1) and (3:1), 100 and 125 μg/mL respectively. Moreover, the Au-MSS/TPGS-PEI and Au-MSS/TPGS/PEI (3:1) formulations were successfully internalized by HeLa cells. Overall, the attained data confirm the successful modification of Au-MSS nanorods with TPGS and PEI polymers. Additionally, the Au-MSS/TPGS-PEI (1 min) formulation showed the most promising properties, followed by Au-MSS/TPGS/PEI (3:1) nanorods, for being applied in cancer chemotherapy, PTT and imaging.

Conflicts of interest

The authors declare no financial or commercial conflict of interest.

Acknowledgements

This work was supported by FEDER funds through the POCI – COMPETE 2020 – Operational Programme Competitiveness and Internationalisation in Axis I – Strengthening research, technological development and innovation (Project POCI-01-0145-FEDER-007491) and National Funds by FCT – Foundation for Science and Technology (Project UID/Multi/00709/2013). The funding from CENTRO-01-0145-FEDER-028989 and POCI-01-0145-FEDER-031462 are also acknowledged. The Applied Molecular Biosciences Unit- UCIBIO acknowledge the funds from FCT/MCTES (UID/Multi/04378/2013) and ERDF under the PT2020 Partnership Agreement (POCI-01-0145-FEDER-007728). André F. Moreira acknowledge their individual Ph.D. fellowship from FCT (SFRH/BD/109482/2015). The funders had no role in the decision to publish or in the preparation of the manuscript.

Appendix A. Supplementary data

Supplementary data related to this article can be found at https://doi.org/10.1016/j.micromeso.2019.04.064.

References

[1] R.L. Siegel, K.D. Miller, A. Jemal, Cancer statistics, CA A Cancer J. Clin. 68 (2018) 7–30 (2018).
[2] M. Rebucci, C. Michiels, Molecular aspects of cancer cell resistance to chemotherapy, Biochem. Pharmacol. 85 (2013) 1219–1226.
[3] I. Brigger, C. Dubernet, P. Couvreur, Nanoparticles in cancer therapy and diagnosis, Adv. Drug Deliv. Rev. 64 (2012) 24–36.
[4] A. Makkouk, G.J. Weiner, Cancer immunotherapy and breaking immune tolerance: new approaches to an old challenge, Cancer Res. 75 (2015) 5–10.
[5] N.R. Datta, S.G. Ordonez, U.S. Gaipl, M.M. Paulides, H. Crezee, J. Gellermann, D. Marder, E. Puric, S. Bodis, Local hyperthermia combined with radiotherapy and-/or chemotherapy: recent advances and promises for the future, Cancer Treat Rev. 41 (2015) 742–753.
[6] N. Cihoric, A. Tsikkinis, G. van Rhoon, H. Crezee, D.M. Aebersold, S. Bodis, M. Beck, J. Nadobny, V. Budach, P. Wust, P. Ghadjar, Hyperthermia-related clinical trials on cancer treatment within the ClinicalTrials.gov registry, Int. J. Hyperth. 31 (2015) 609–614.
[7] J.R. Melamed, R.S. Edelstein, E.S. Day, Elucidating the fundamental mechanisms of cell death triggered by photothermal therapy, ACS Nano 9 (2015) 6–11.
[8] J. Beik, Z. Abed, F.S. Ghoreishi, S. Hosseini-Nami, S. Mehrzadi, A. Shakeri-Zadeh, S.K. Kamrava, Nanotechnology in hyperthermia cancer therapy: from fundamental principles to advanced applications, J. Control. Release 235 (2016) 205–221.
[9] D. de Melo-Diogo, C. Pais-Silva, E.C. Costa, R.O. Louro, I.J. Correia, D-alpha-tocopheryl polyethylene glycol 1000 succinate functionalized nanographene oxide for cancer therapy, Nanomedicine (Lond) 12 (2017) 443–456.
[10] D.R. Dias, A.F. Moreira, I.J. Correia, The effect of the shape of gold core-mesoporous silica shell nanoparticles on the cellular behavior and tumor spheroid penetration, J. Mater. Chem. B 4 (2016) 7630–7640.
[11] J.L. Geng, C.Y. Sun, J. Liu, L.D. Liao, Y.Y. Yuan, N. Thakor, J. Wang, B. Liu, Biocompatible conjugated polymer nanoparticles for efficient photothermal tumor therapy, Small 11 (2015) 1603–1610.
[12] C. Pais-Silva, D. de Melo-Diogo, I.J. Correia, IR780-loaded TPGS-TOS micelles for breast cancer photodynamic therapy, Eur. J. Pharm. Biopharm. 113 (2017) 108–117.
[13] A.M. Alkilany, L.B. Thompson, S.P. Boulos, P.N. Sisco, C.J. Murphy, Gold nanorods: their potential for photothermal therapeutics and drug delivery, tempered by the complexity of their biological interactions, Adv. Drug Deliv. Rev. 64 (2012) 190–199.
[14] A. Popovtzer, A. Mizrachi, M. Motiei, D. Bragilovski, L. Lubimov, M. Levi, O. Hilly, I. Ben-Aharon, R. Popovtzer, Actively targeted gold nanoparticles as novel

radiosensitizer agents: an in vivo head and neck cancer model, Nanoscale 8 (2016) 2678–2685.
[15] J. Lee, D.K. Chatterjee, M.H. Lee, S. Krishnan, Gold nanoparticles in breast cancer treatment: promise and potential pitfalls, Cancer Lett. 347 (2014) 46–53.
[16] S.B. Lee, H.W. Lee, T.D. Singh, Y. Li, S.K. Kim, S.J. Cho, S.W. Lee, S.Y. Jeong, B.C. Ahn, S. Choi, I.K. Lee, D.K. Lim, J. Lee, Y.H. Jeon, Visualization of macrophage recruitment to inflammation lesions using highly sensitive and stable radionuclide-embedded gold nanoparticles as a nuclear bio-imaging platform, Theranostics 7 (2017) 926–934.
[17] L.J. Jing, X.L. Liang, Z.J. Deng, S.S. Feng, X.D. Li, M.M. Huang, C.H. Li, Z.F. Dai, Prussian blue coated gold nanoparticles for simultaneous photoacoustic/CT bimodal imaging and photothermal ablation of cancer, Biomaterials 35 (2014) 5814–5821.
[18] X. Cheng, R. Sun, L. Yin, Z. Chai, H. Shi, M. Gao, Light-triggered assembly of gold nanoparticles for photothermal therapy and photoacoustic imaging of tumors in vivo, Adv. Mater. 29 (2017).
[19] J. Zhang, C. Li, X. Zhang, S. Huo, S. Jin, F.F. An, X. Wang, X. Xue, C.I. Okeke, G. Duan, F. Guo, X. Zhang, J. Hao, P.C. Wang, J. Zhang, X.J. Liang, In vivo tumor-targeted dual-modal fluorescence/CT imaging using a nanoprobe co-loaded with an aggregation-induced emission dye and gold nanoparticles, Biomaterials 42 (2015) 103–111.
[20] J.Y. Liu, Q.A. Peng, Protein-gold nanoparticle interactions and their possible impact on biomedical applications, Acta Biomater. 55 (2017) 13–27.
[21] J.C. Love, L.A. Estroff, J.K. Kriebel, R.G. Nuzzo, G.M. Whitesides, Self-assembled monolayers of thiolates on metals as a form of nanotechnology, Chem. Rev. 105 (2005) 1103–1169.
[22] X.H. Huang, P.K. Jain, I.H. El-Sayed, M.A. El-Sayed, Gold nanoparticles: interesting optical properties and recent applications in cancer diagnostic and therapy, Nanomedicine 2 (2007) 681–693.
[23] G. Jalani, M. Cerruti, Nano graphene oxide-wrapped gold nanostars as ultrasensitive and stable SERS nanoprobes, Nanoscale 7 (2015) 9990–9997.
[24] Y.S. Chen, W. Frey, S. Kim, K. Homan, P. Kruizinga, K. Sokolov, S. Emelianov, Enhanced thermal stability of silica-coated gold nanorods for photoacoustic imaging and image-guided therapy, Optic Express 18 (2010) 8867–8877.
[25] H. Li, L.L. Tan, P. Jia, Q.L. Li, Y.L. Sun, J. Zhang, Y.Q. Ning, J.H. Yu, Y.W. Yang, Near-infrared light-responsive supramolecular nanovalve based on mesoporous silica-coated gold nanorods, Chem. Sci. 5 (2014) 2804–2808.
[26] J. Lipka, M. Semmler-Behnke, R.A. Sperling, A. Wenk, S. Takenaka, C. Schleh, T. Kissel, W.J. Parak, W.G. Kreyling, Biodistribution of PEG-modified gold nanoparticles following intratracheal instillation and intravenous injection, Biomaterials 31 (2010) 6574–6581.
[27] J. Gao, X.Y. Huang, H. Liu, F. Zan, J.C. Ren, Colloidal stability of gold nanoparticles modified with thiol compounds: bioconjugation and application in cancer cell imaging, Langmuir 28 (2012) 4464–4471.
[28] C.Y. Li, Z.J. Liu, P. Yao, Gold nanoparticles coated with a polydopamine layer and dextran brush surface for diagnosis and highly efficient photothermal therapy of tumors, RSC Adv. 6 (2016) 33083–33091.
[29] W.G. Kreyling, A.M. Abdelmonem, Z. Ali, F. Alves, M. Geiser, N. Haberl, R. Hartmann, S. Hirn, D.J. de Aberasturi, K. Kantner, G. Khadem-Saba, J.M. Montenegro, J. Rejman, T. Rojo, I.R. de Larramendi, R. Ufartes, A. Wenk, W.J. Parak, In vivo integrity of polymer-coated gold nanoparticles, Nat. Nanotechnol. 10 (2015) 619(-+).
[30] J. Liu, C. Detrembleur, M.C. De Pauw-Gillet, S. Mornet, C. Jerome, E. Duguet, Gold nanorods coated with mesoporous silica shell as drug delivery system for remote near infrared light-activated release and potential phototherapy, Small 11 (2015) 2323–2332.
[31] A. Khanal, C. Ullum, C.W. Kimbrough, N.C. Garbett, J.A. Burlison, M.W. McNally, P. Chuong, A.S. El-Baz, J.B. Jasinski, L.R. McNally, Tumor targeted mesoporous silica-coated gold nanorods facilitate detection of pancreatic tumors using Multispectral optoacoustic tomography, Nano Res 8 (2015) 3864–3877.
[32] M. Kar, N. Tiwari, M. Tiwari, M. Lahiri, S. Sen Gupta, Poly-l-arginine grafted silica mesoporous nanoparticles for enhanced cellular uptake and their application in DNA delivery and controlled drug release, Part. Part. Syst. Char. 30 (2013) 166–179.
[33] V. Mamaeva, C. Sahlgren, M. Linden, Mesoporous silica nanoparticles in medicine-Recent advances, Adv. Drug Deliv. Rev. 65 (2013) 689–702.
[34] J.T. Song, X.Q. Yang, X.S. Zhang, D.M. Yang, Z.Y. Wang, Y.D. Zhao, Facile synthesis of gold nanospheres modified by positively charged mesoporous silica, loaded with near-infrared fluorescent dye, for in vivo X-ray computed tomography and fluorescence dual mode imaging, ACS Appl. Mater. Interfaces 7 (2015) 17287–17297.
[35] R.G. Chaudhuri, S. Paria, Core/shell nanoparticles: classes, properties, synthesis mechanisms, characterization, and applications, Chem. Rev. 112 (2012) 2373–2433.
[36] M. Kanehara, Y. Watanabe, T. Teranishi, Thermally stable silica-coated hydrophobic gold nanoparticles, J. Nanosci. Nanotechnol. 9 (2009) 673–675.
[37] J.C. Chen, R.Y. Zhang, L. Han, B. Tu, D.Y. Zhao, One-pot synthesis of thermally stable gold@mesoporous silica core-shell nanospheres with catalytic activity, Nano Res 6 (2013) 871–879.
[38] I.I. Slowing, B.G. Trewyn, S. Giri, V.S.Y. Lin, Mesoporous silica nanoparticles for drug delivery and biosensing applications, Adv. Funct. Mater. 17 (2007) 1225–1236.
[39] A.F. Moreira, D.R. Dias, I.J. Correia, Stimuli-responsive mesoporous silica nanoparticles for cancer therapy: a review, Microporous Mesoporous Mater. 236 (2016) 141–157.
[40] R. Cheng, F.H. Meng, C. Deng, H.A. Klok, Z.Y. Zhong, Dual and multi-stimuli responsive polymeric nanoparticles for programmed site-specific drug delivery, Biomaterials 34 (2013) 3647–3657.
[41] C.L. Yang, T.T. Wu, Y. Qi, Z.P. Zhang, Recent advances in the application of vitamin E TPGS for drug delivery, Theranostics 8 (2018) 464–485.
[42] Z.P. Zhang, S.W. Tan, S.S. Feng, Vitamin E TPGS as a molecular biomaterial for drug delivery, Biomaterials 33 (2012) 4889–4906.
[43] P.Y. Li, P.S. Lai, W.C. Hung, W.J. Syu, Poly(L-lactide)-Vitamin E TPGS nanoparticles enhanced the cytotoxicity of doxorubicin in drug-resistant MCF-7 breast cancer cells, Biomacromolecules 11 (2010) 2576–2582.
[44] G. Jiang, K. Park, J. Kim, K.S. Kim, E.J. Oh, H.G. Kang, S.E. Han, Y.K. Oh, T.G. Park, S.K. Hahn, Hyaluronic acid-polyethyleneimine conjugate for target specific intracellular delivery of siRNA, Biopolymers 89 (2008) 635–642.
[45] A.F. Moreira, D.R. Dias, E.C. Costa, I.J. Correia, Thermo- and pH-responsive nano-in-micro particles for combinatorial drug delivery to cancer cells, Eur. J. Pharm. Sci. 104 (2017) 42–51.
[46] A.F. Moreira, V.M. Gaspar, E.C. Costa, D. de Melo-Diogo, P. Machado, C.M. Paquete, I.J. Correia, Preparation of end-capped pH-sensitive mesoporous silica nanocarriers for on-demand drug delivery, Eur. J. Pharm. Biopharm. 88 (2014) 1012–1025.
[47] J. Shen, Q. Yin, L. Chen, Z. Zhang, Y. Li, Co-delivery of paclitaxel and survivin shRNA by pluronic P85-PEI/TPGS complex nanoparticles to overcome drug resistance in lung cancer, Biomaterials 33 (2012) 8613–8624.
[48] M. Schroeder, H.B. Lenting, A. Kandelbauer, C.J. Silva, A. Cavaco-Paulo, G.M. Gubitz, Restricting detergent protease action to surface of protein fibres by chemical modification, Appl. Microbiol. Biotechnol. 72 (2006) 738–744.
[49] A. Khatibi, L. Ma'mani, R. Khodarahmi, A. Shafiee, P. Maghami, F. Ahmad, N. Sheibani, A.A. Moosavi-Movahedi, Enhancement of thermal reversibility and stability of human carbonic anhydrase II by mesoporous nanoparticles, Int. J. Biol. Macromol. 75 (2015) 67–72.
[50] Q.J. He, J.M. Zhang, J.L. Shi, Z.Y. Zhu, L.X. Zhang, W.B. Bu, L.M. Guo, Y. Chen, The effect of PEGylation of mesoporous silica nanoparticles on nonspecific binding of serum proteins and cellular responses, Biomaterials 31 (2010) 1085–1092.
[51] A. Yildirim, E. Ozgur, M. Bayindir, Impact of mesoporous silica nanoparticle surface functionality on hemolytic activity, thrombogenicity and non-specific protein adsorption, J. Mater. Chem. B 1 (2013) 1909–1920.
[52] A.F. Moreira, V.M. Gaspar, E.C. Costa, D. de Melo-Diogo, P. Machado, C.M. Paquete, I.J. Correia, Preparation of end-capped pH-sensitive mesoporous silica nanocarriers for on-demand drug delivery, Eur. J. Pharm. Biopharm. 88 (2014) 1012–1025.
[53] A.F. Moreira, C.F. Rodrigues, C.A. Reis, E.C. Costa, P. Ferreira, I.J. Correia, Development of poly-2-ethyl-2-oxazoline coated gold-core silica shell nanorods for cancer chemo-photothermal therapy, Nanomedicine 13 (2018).
[54] V.M. Gaspar, A.F. Moreira, E.C. Costa, J.A. Queiroz, F. Sousa, C. Pichon, I.J. Correia, Gas-generating TPGS-PLGA microspheres loaded with nanoparticles (NIMPS) for co-delivery of minicircle DNA and anti-tumoral drugs, Colloids Surf., B 134 (2015) 287–294.
[55] Y. Wu, Q. Chu, S. Tan, X. Zhuang, Y. Bao, T. Wu, Z. Zhang, D-α-tocopherol polyethylene glycol succinate-based derivative nanoparticles as a novel carrier for paclitaxel delivery, Int. J. Nanomed. 10 (2015) 5219.
[56] B. Nikoobakht, M.A. El-Sayed, Preparation and growth mechanism of gold nanorods (NRs) using seed-mediated growth method, Chem. Mater. 15 (2003) 1957–1962.
[57] I. Gorelikov, N. Matsuura, Single-step coating of mesoporous silica on cetyltrimethyl ammonium bromide-capped nanoparticles, Nano Lett. 8 (2008) 369–373.
[58] S.W. Wang, W. Xi, F.H. Cai, X.Y. Zhao, Z.P. Xu, J. Qian, S.L. He, Three-photon luminescence of gold nanorods and its applications for high Contrast tissue and deep in vivo brain imaging, Theranostics 5 (2015) 251–266.
[59] X. Huang, M.A. El-Sayed, Gold nanoparticles: optical properties and implementations in cancer diagnosis and photothermal therapy, J. Adv. Res. 1 (2010) 13–28.
[60] J. Becker, A. Trugler, A. Jakab, U. Hohenester, C. Sonnichsen, The optimal aspect ratio of gold nanorods for plasmonic bio-sensing, Plasmonics 5 (2010) 161–167.
[61] E. Frohlich, The role of surface charge in cellular uptake and cytotoxicity of medical nanoparticles, Int. J. Nanomed. 7 (2012) 5577–5591.
[62] R.K. Jain, T. Stylianopoulos, Delivering nanomedicine to solid tumors, Nat. Rev. Clin. Oncol. 7 (2010) 653–664.
[63] M. Roser, D. Fischer, T. Kissel, Surface-modified biodegradable albumin nano- and microspheres. II: effect of surface charges on in vitro phagocytosis and biodistribution in rats, Eur. J. Pharm. Biopharm. 46 (1998) 255–263.
[64] B.S. Kim, C.S. Kim, K.M. Lee, The intracellular uptake ability of chitosan-coated poly (D,L-lactide-co-glycolide) nanoparticles, Arch Pharm. Res. (Seoul) 31 (2008) 1050–1054.
[65] J. Kobler, K. Moller, T. Bein, Colloidal suspensions of functionalized mesoporous silica nanoparticles, ACS Nano 2 (2008) 791–799.
[66] J.M. Kim, S.M. Chang, S.M. Kong, K.S. Kim, J. Kim, W.S. Kim, Control of hydroxyl group content in silica particle synthesized by the sol-precipitation process, Ceram. Int. 35 (2009) 1015–1019.
[67] J. Eichler, J. Knof, H. Lenz, Measurements on the depth of penetration of light (0.35–1.0 μm) in tissue, Radiat. Environ. Biophys. 14 (1977) 239–242.
[68] S. Stolik, J. Delgado, A. Perez, L. Anasagasti, Measurement of the penetration depths of red and near infrared light in human “ex vivo” tissues, J. Photochem. Photobiol. B Biol. 57 (2000) 90–93.
[69] M. Lequeux, J. Grand, G. Laurent, Importance of gold nanorods' aggregation in surface plasmon coupling with a photochromic film in hybrid structures, Plasmonics 10 (2015) 1863–1868.
[70] S.F. Du, K. Kendall, P. Toloueinia, Y. Mehrabadi, G. Gupta, J. Newton, Aggregation and adhesion of gold nanoparticles in phosphate buffered saline, J. Nano Res. 14 (2012).
[71] Q.H. Zeng, Y.L. Zhang, W.Y. Ji, W.G. Ye, Y.L. Jiang, J. Song, Inhibitation of cellular toxicity of gold nanoparticles by surface encapsulation of silica shell for hepatocarcinoma cell application, ACS Appl. Mater. Interfaces 6 (2014) 19327–19335.

[72] C.M. Neophytou, C. Constantinou, P. Papageorgis, A.I. Constantinou, D-alpha-tocopheryl polyethylene glycol succinate (TPGS) induces cell cycle arrest and apoptosis selectively in Survivin-overexpressing breast cancer cells, Biochem. Pharmacol. 89 (2014) 31–42.

[73] Z. Zhang, L. Wang, J. Wang, X. Jiang, X. Li, Z. Hu, Y. Ji, X. Wu, C. Chen, Mesoporous silica-coated gold nanorods as a light-mediated multifunctional theranostic platform for cancer treatment, Adv. Mater. 24 (2012) 1418–1423.

[74] P. Huang, L. Bao, C. Zhang, J. Lin, T. Luo, D. Yang, M. He, Z. Li, G. Gao, B. Gao, Folic acid-conjugated silica-modified gold nanorods for X-ray/CT imaging-guided dual-mode radiation and photo-thermal therapy, Biomaterials 32 (2011) 9796–9809.